Cell Reports
Physical Science

CellPress
OPEN ACCESS

Article

Comparing the reaction profiles of single iron catalytic sites in enzymes and in reticular frameworks for methane-to-methanol oxidation

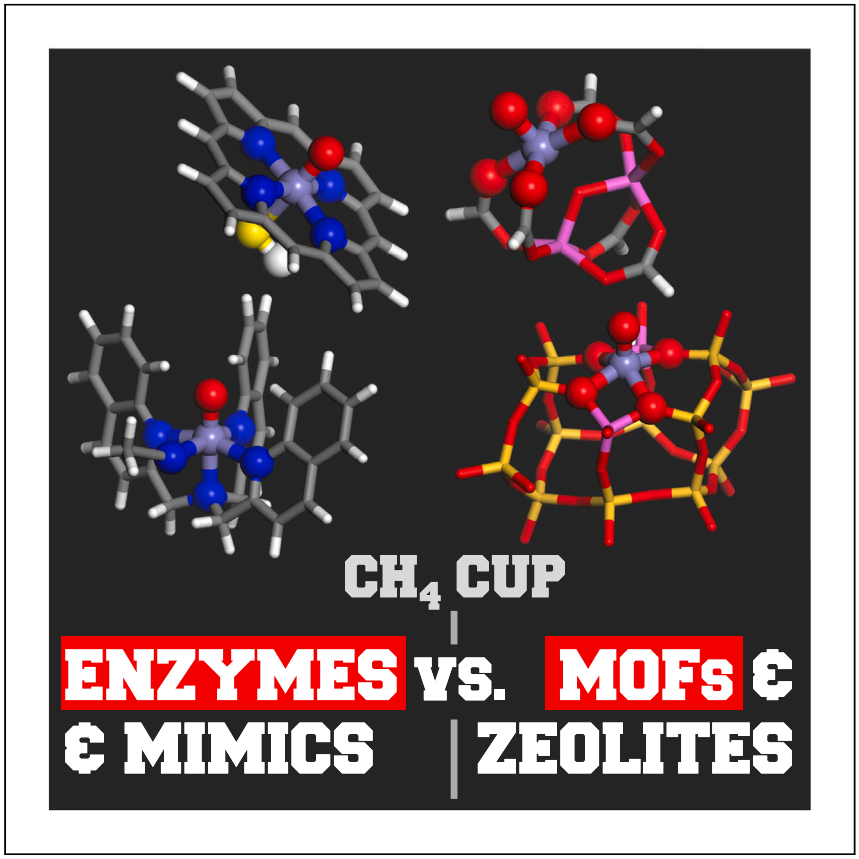

Here, Vitillo et al. exploit computational methods to compare iron active sites in biomimetic models and reticular framework-based catalysts for the methane-to-methanol reaction. Using first coordination shell cluster models, they identify key targets for the next generation of zeolite and metal-organic framework-based synthetic catalysts.

Jenny G. Vitillo, Connie C. Lu, Aditya Bhan, Laura Gagliardi

jg.vitillo@gmail.com

Highlights

Iron-containing biomimetic and synthetic catalysts are compared using Kohn-Sham DFT

A zeolite shows lower activation barriers than enzymes for methane-to-methanol conversion

The first coordination shell of iron impacts methanol selectivity only to a limited extent

Methanol protectors in the microenvironment are mandatory to achieve high selectivity

Vitillo et al., Cell Reports Physical Science 4, 101422
June 21, 2023
https://doi.org/10.1016/j.xcrp.2023.101422

Please cite this article in press as: Vitillo et al., Comparing the reaction profiles of single iron catalytic sites in enzymes and in reticular frameworks for methane-to-methanol oxidation, Cell Reports Physical Science (2023), https://doi.org/10.1016/j.xcrp.2023.101422

Cell Reports
Physical Science

Article

Comparing the reaction profiles of single iron catalytic sites in enzymes and in reticular frameworks for methane-to-methanol oxidation

Jenny G. Vitillo,[1,5,8,*] Connie C. Lu,[2,6] Aditya Bhan,[3] and Laura Gagliardi[4,7]

SUMMARY

The design of synthetic inorganic catalysts mimicking the first coordination spheres of enzymatic cofactors often results in lower yields and selectivity than their biological counterparts. In this study, we exploit Kohn-Sham density functional methods to compare the reaction profiles of four single iron-based catalysts for the direct oxidation of methane to methanol: two biomimetic models based on two enzymes (cytochrome P450 and taurine dioxygenase [TauD]) and two synthetic reticular frameworks (iron-BEA zeolite and tri-iron oxo-center-based metal-organic framework). Both the biomimetic and inorganic catalysts show almost zero selectivity toward methanol for methane conversions >1% at ambient temperature. This study highlights that iron's first coordination shell can influence selectivity toward methanol but to a limited extent. In the absence of methanol protection strategies, high selectivity can be reached only by mimicking the reaction microenvironment of enzymes beyond the first coordination shell of iron.

INTRODUCTION

Enzymes are able to catalyze a wide variety of reactions necessary for metabolic processes in biological systems with high selectivity, high turnover frequencies,[1] and often at ambient temperature and pressure conditions.[2] Nevertheless, industrial application of enzymes is hindered in several cases by their limited thermal stability, difficulty in product separation, and the complexity of the whole biological environment that cooperates with the metallic active site in the enzyme to execute a specific function.[1]

Enzyme-inspired catalysts, or synthetic catalysts that mimic the enzymatic active site, aim to couple the activity and selectivity of enzymes with characteristics more suitable for industrial applications. Several thousand biomimetic catalysts have been reported. Among them, synthetic enzymes[3] and homogeneous complexes retain often the same catalytic activity but also stability and separation issues of the corresponding enzymes.[2] Metal complexes as part of high surface area materials, like metal-organic frameworks (MOFs) and zeolites, are sought as a way to solve these issues, despite sometimes showing lower reactivity and selectivity.[2]

C–H bond activation is an important reaction for several biological and synthetic processes. Among these processes, the direct oxidation of methane to methanol (MTM) is considered the most challenging but also the most rewarding reaction in terms of economic and environmental repercussions.[4] Iron- and copper-containing redox cofactors in enzymes are still, after several decades of research, the best

[1]Department of Science and High Technology and INSTM, Università degli Studi dell'Insubria, Via Valleggio 9, 22100 Como, Italy

[2]Institute of Inorganic Chemistry, University of Bonn, Gerhard-Domagk-Str. 1, 53121 Bonn, Germany

[3]Department of Chemical Engineering and Materials Science, University of Minnesota, 421 Washington Avenue S.E., Minneapolis, MN 55455, USA

[4]Department of Chemistry, Pritzker School of Molecular Engineering, James Franck Institute, University of Chicago, Chicago, IL 60637, USA

[5]Twitter: @JVitillo

[6]Twitter: @cluchem

[7]Twitter: @gagliardi8

[8]Lead contact

*Correspondence: jg.vitillo@gmail.com

https://doi.org/10.1016/j.xcrp.2023.101422

Please cite this article in press as: Vitillo et al., Comparing the reaction profiles of single iron catalytic sites in enzymes and in reticular frameworks for methane-to-methanol oxidation, Cell Reports Physical Science (2023), https://doi.org/10.1016/j.xcrp.2023.101422

catalysts in this field.[2] It is clear from recent literature that selectivity is the characteristic that is most lacking for synthetic catalysts in reference to their enzymatic counterparts.[2,4,5] This is not surprising: the lower C–H bond dissociation energy in methanol (402.1 kJ mol^{-1})[6] than in methane (439.3 kJ mol^{-1})[6] makes methanol overoxidation likely unless strategies aimed at protecting methanol are leveraged.[4,5,7] It is an established concept in metalloproteins that the reactivity and, even more, the selectivity of enzymes are mainly related to components external to the metal and its first coordination sphere,[8] like non-covalent interactions[9–15] and diffusion characteristics.[11,16,17] These elements are related to the structure and reaction environment that circumscribes the metallic active site in enzymes, with several building blocks contributing to tailor optimally the enzyme toward a very specific function.[11,18–21] Nevertheless, from recent reviews comparing bioinorganic and inorganic catalysts for C–H bond activation reactions,[2,4,22,23] it is hard to understand if the higher selectivity and methane conversion achieved by enzymes are determined by the first coordination sphere of the metal and to what extent. This question is of upmost importance because the biomimetic approach in synthetic catalyst design is often limited to the first coordination shell around the metal.

The reaction conditions are another important aspect that can make a difference. The reaction medium is a common variable in catalysis used to improve both the selectivity and conversion.[8,11,24] Solvents can directly influence the reaction profile,[11,19,25,26] or they can act as protecting agents of the unstable products.[5,27] Zeolites and MOFs are often tested in the gas phase,[7,17,28–31] while enzymes classically work in solution: this difference can increase the selectivity for enzymes, making the comparison uneven. Moreover, from the computational point of view, different levels of approximation used in studies limit the comparison.[32]

In this study, we have used Kohn-Sham density functional theory (KS-DFT) calculations to compare the reaction profiles and the selectivity of four single-site, iron-based catalysts for MTM: two biomimetic models based on two enzymes and two synthetic heterogeneous catalysts. A cluster approach was used in which only the iron and its first coordination sphere were considered. Reaction conditions adopted in the testing of single-site iron heterogeneous catalysts—gas phase, ambient pressure, and ambient temperature—were studied. N_2O was considered the oxygen source. In heterogeneous catalysts, N_2O is often preferred over other oxygen sources (i.e., O_2), as it yields higher selectivity in the formation of iron-oxo species for reactions in the gas phase.[4,30,33] Identical reaction conditions and having clusters restricted only to the metal and its first coordination shell allow us to directly relate the differences in the reaction profiles and selectivity among the catalysts to the local structure shown in Figure 1. The results of this study are that, when considering only the first coordination sphere, enzymes perform poorly in reference to existing catalysts based on reticular frameworks for the MTM reaction. Specifically, we find that a synthetic catalyst, Fe-BEA*, is superior to P450 for the MTM reaction when only considering the first coordination sphere. This is a surprising result, one that contradicts the prevailing literature, because there are few attempts to make an apples-to-apples quantitative comparison between enzymes and reticular framework catalysts.

This rigorous approach enables us to identify straightforwardly the directions needed for the design and development of the next generation of reticular-framework-based MTM catalysts.

Please cite this article in press as: Vitillo et al., Comparing the reaction profiles of single iron catalytic sites in enzymes and in reticular frameworks for methane-to-methanol oxidation, Cell Reports Physical Science (2023), https://doi.org/10.1016/j.xcrp.2023.101422

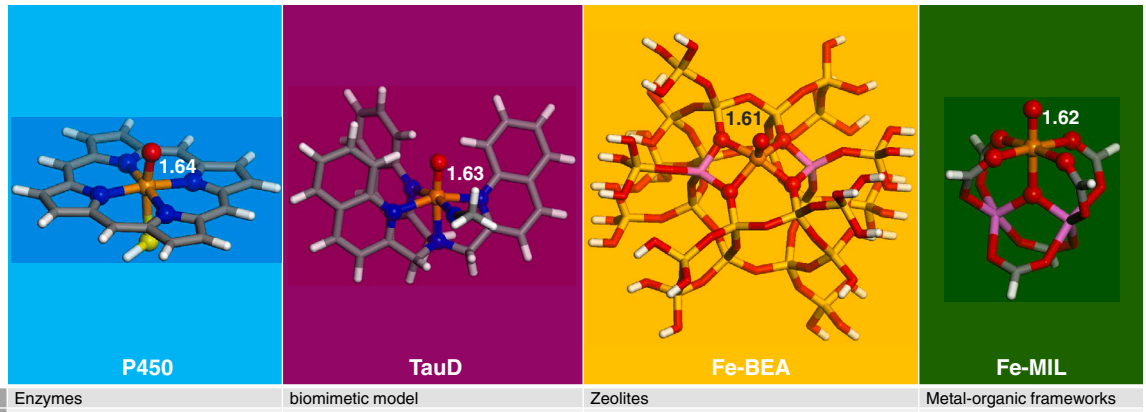

	P450	TauD	Fe-BEA	Fe-MIL
Class	Enzymes	biomimetic model	Zeolites	Metal-organic frameworks
Iron site type	heme	non-heme	non-heme	non-heme
Reduced form	HS Fe(III)	HS Fe(II)	HS Fe(II)	HS Fe(II)
Active form	LS Fe(IV)=O	HS Fe(IV)=O	HS Fe(IV)=O	HS Fe(IV)=O
Single- or two-state reactivity	Both	Single-state	Single-state	Single-state
Selectivity	High	High	High	Low
Reaction medium[a]	Solution	Solution	Gas phase, solution[b]	Gas phase, solution[b]
Tested for MTM[a]	No	No	Yes, at RT	Yes, at 90 °C

[a]in experiments. [b]conditions not used for MTM

Figure 1. Identity card of the cluster models used for the active form of the single-site iron catalysts considered in this study

The M06-L/def2-TZVP structure of the models is reported in the top part of the figure along with the oxoferryl bond distance (Å) for the sake of comparison (B clusters in Scheme 1 after the removal of N_2). HS, high spin; LS, low spin. Color code: red (oxygen), orange (iron), blue (nitrogen), bright yellow (sulfur), dark yellow (silicon), magenta (aluminum), gray (carbon), white (hydrogen).

RESULTS AND DISCUSSION

Consideration for comparison

The reaction cycle followed is the one reported in Scheme 1. It is composed of four steps[34]: (1) N_2O adsorption on the iron center and dissociation to form N_2 and the ferryl (from **A**N_2**O** to **B**)[17,29,35]; (2) interaction of methane with the oxo-species and dissociation of one C–H bond resulting in a methyl radical and a hydroxo group on the iron (from **C** to **D**)[9,34–36]; (3) radical rebound between the methyl radical and the hydroxo species, forming methanol (from **D** to **E**)[9,36,37]; and (4) methanol desorption and regeneration of the catalytic center (from **E** to **A**).

Methanol selectivity has been quantified using the kinetic model reported by Latimer et al.[5] This model assumes that hydrogen abstraction (**C** to **D** step in Scheme 1) is rate determining in both methane and methanol cycles. It also assumes that no protection mechanisms of methanol are operating. The selectivity so obtained represents, then, an upper bond of the selectivity at a given conversion, but it has proven to be a useful parameter when comparing different classes of MTM catalysts (for more details, please refer to Latimer et al.[5] and for further discussion, *vide infra*).

For the enzymatic systems, we considered cytochrome P450 and taurine dioxygenase (TauD). Cytochromes P450 are a class of enzymes that catalyze a large set of diverse reactions in biological systems, the most common involving a single oxygen insertion (monooxygenate enzyme).[9,39] The metal center of P450 is a heme Fe site (iron(III) protoporphyrin IX) with cysteinate as the axial ligand.[9,18,40] The catalytic species in its active form is often indicated as compound I (Cpd I in the following; see blue panel in Figure 1 for the model used).

The Fe(II)/α-ketoglutarate (αKG)-dependent dioxygenases is a large family of non-heme enzymes that are pivotal in many metabolic processes.[41] In this case, the metal center is constituted by a single high-spin Fe(II) that needs to be oxidized to be

Please cite this article in press as: Vitillo et al., Comparing the reaction profiles of single iron catalytic sites in enzymes and in reticular frameworks for methane-to-methanol oxidation, Cell Reports Physical Science (2023), https://doi.org/10.1016/j.xcrp.2023.101422

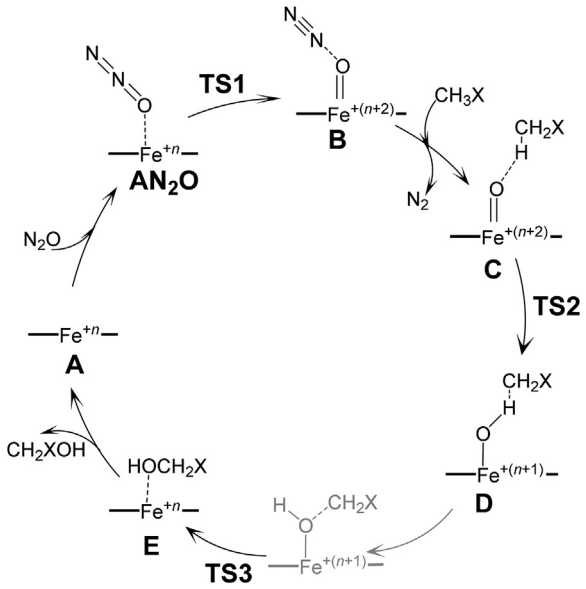

Scheme 1. Computed catalytic cycles for methane and methanol oxidation

Catalytic cycles for methane-to-methanol (X = H) and methanol-to-methylene glycol (X = OH) reactions considered in this study. The formal oxidation state of iron, $+n$, with $n = 3$ for P450[9] and $n = 2$ for TauD,[36,38] Fe-BEA,[17] and Fe-MIL.[35] A similar cycle was used for the conversion of methanol to methanediol. Only the labeled structures in the cycle were considered in the present work. The part of the cycle considered in the present work is reported in dark black.

transformed into the catalytic active species, a high-spin Fe(IV)-oxo.[22,36] TauD (taurine/α-KG dioxygenase) is the most widely studied member of this enzyme family.[36,42,38] Biswas et al.[38] have recently reported a model complex that, although differing in the number of the ligands in the first coordination shell of iron, is able to reproduce the functional and electronic properties of TauD in its active form. This biomimetic model is reported in the second column in Figure 1, and it is the system that we have included in this comparative study.

Among the synthetic inorganic heterogeneous catalysts, α-Fe sites in zeolites are the only synthetic metal species able to catalyze the MTM reaction at ambient temperature. These sites are particularly abundant in the Beta (*BEA framework)[2,17,30] and Chabazite zeolites (CHA framework).[31] We have then included Fe-BEA* in our study, being the most active among synthetic catalysts reported to date. Recently, after decades of debate about the nuclearity of the metal in the catalytic center,[30,43] the structure of the α-Fe in iron zeolites has been unambiguously defined as a single-site, high-spin, non-heme iron (see Figure 1).[2,17] The active species, α-O, are the result of N_2O or O_2 decomposition on the single-site species, α-Fe(II), created by high temperature activation of the sample (removal of adsorbates in vacuum or inert atmosphere). This α-O (or α-Fe) is a single-metal, high-spin Fe(IV)=O species (see third column in Figure 1).

Several MOFs have been reported to catalyze C–H bond activation.[34,44–49] Tri-iron oxo-centered clusters (formula: $[Fe(III)_3(\mu_3\text{-}O)(X)]^{6+}$, with X = OH, F, Cl) are present as secondary building units in several MOFs (e.g., MIL-100,[50] MIL-127,[51] CUB-30,[52] …). In these materials, after removal of the X group from the cluster, one of the tri-valent irons is reduced to Fe(II). This center can be converted by N_2O decomposition to a single-site (non-heme) Fe(IV)=O (see fourth column in Figure 1 for the model used). Oxoferryl species in MIL-100(Fe) and MIL-127(Fe) have been shown to

catalyze C–H activation in methane at 90°C and 1 bar.[7] The high thermal and chemical stability of the MOFs based on these metal clusters allow the materials to be stable under oxidative conditions. These characteristics make these MOFs the best catalyst nowadays for the MTM reaction among the reported iron-based MOFs.[34,44–49] We have then included the tri-iron oxo-centered cluster as representative of synthetic catalysts in the set used in this study.

We would like to stress that our aim is not to reproduce with high accuracy the reactivity of these catalysts in the MTM reaction in the different reaction conditions adopted experimentally for each of them. These points have been addressed in previous experiments or computational studies by using larger clusters and molecular dynamics. Here, the target is to understand how risky the typical strategy used in designing new catalysts based on reticular frameworks is by limiting the mimicking approach only to the first coordination sphere of enzymatic cofactors. This being a comparative study, we chose the same reaction conditions for all the catalysts because the conditions can influence the selectivity of the reaction. Because this study is performed in the research field of the design of new reticular frameworks-based catalysts, we have chosen those frequently adopted for catalysts based on reticular frameworks.[7,17,28,44,53]

Ground spin state of the catalysts

For TauD, Fe-BEA, and Fe-MIL, the most stable electronic configuration corresponds to the high spin state, quintet for all the reaction intermediates. The triplet and singlet states lie at significantly higher energy, making these reactions single-state reactions. This outcome agrees with previous DFT and multireference wave function-based studies on these catalysts (see Snyder et al.,[17] Simons et al.,[29] Vitillo et al.,[35] and Biswas et al.[38] and Note S10). For this reason, only their quintet potential energy surfaces will be discussed in the following.

The oxidation state and the spin state of Fe in Cpd I have been debated for a long time.[9,37,39,54] This is due to the small energy difference among the $2S+1 = 2$, 4, and 6 configurations, which can be <2 kJ mol^{-1}.[37,55] Rittle and Green[56] have unambiguously assigned the spin of Cpd I to $S_{total} = 1/2$, with the $S = 1$ Fe(IV) center coupling antiferromagnetically to the unpaired electron in the porphyrin ($S = 1/2$), using electron paramagnetic resonance (EPR) and Mössbauer spectroscopies. Nevertheless, considering a Boltzmann distribution, the small difference in energy would make the three lower spin states of Cpd I all populated at ambient conditions; that is, the doublet, quartet, and sextet forms can be present at the same time in the reaction environment.[54,57,58] Moreover, P450 spin energy surfaces for the different spin states do not remain parallel along the reaction cycles.[9,54,55,57,59] The ground states for P450 reagent state (**A** in Scheme 1) and its oxo-species (**AB**, i.e., **B** in Scheme 1 after the removal of N_2) are the sextet and the doublet, respectively, according to the present work (see Tables S1 and S2) and previous studies.[9,39,54,57,60] In particular **AB-P450** has been extensively studied in the literature using multireference calculations.[9,54,55,59,61,62] The relative energy stability of **AB-P450** on the spin states is doublet < ≈quartet < sextet at the M06-L level, in agreement with previous multireference calculations.[9,54,55,59] This means that the spin energy surfaces (can) undergo spin crossover as the reaction proceeds.[9,39] P450 doublet and the quartet spin states are nearly isoenergetic, depending on whether the unpaired electron on the porphyrin π-cation radical is ferromagnetically or antiferromagnetically coupled to the triplet iron center,[18] with the antiferromagnetic configuration only slightly more stable than the ferromagnetic configuration in **A** and **AB**.[54] For these

Please cite this article in press as: Vitillo et al., Comparing the reaction profiles of single iron catalytic sites in enzymes and in reticular frameworks for methane-to-methanol oxidation, Cell Reports Physical Science (2023), https://doi.org/10.1016/j.xcrp.2023.101422

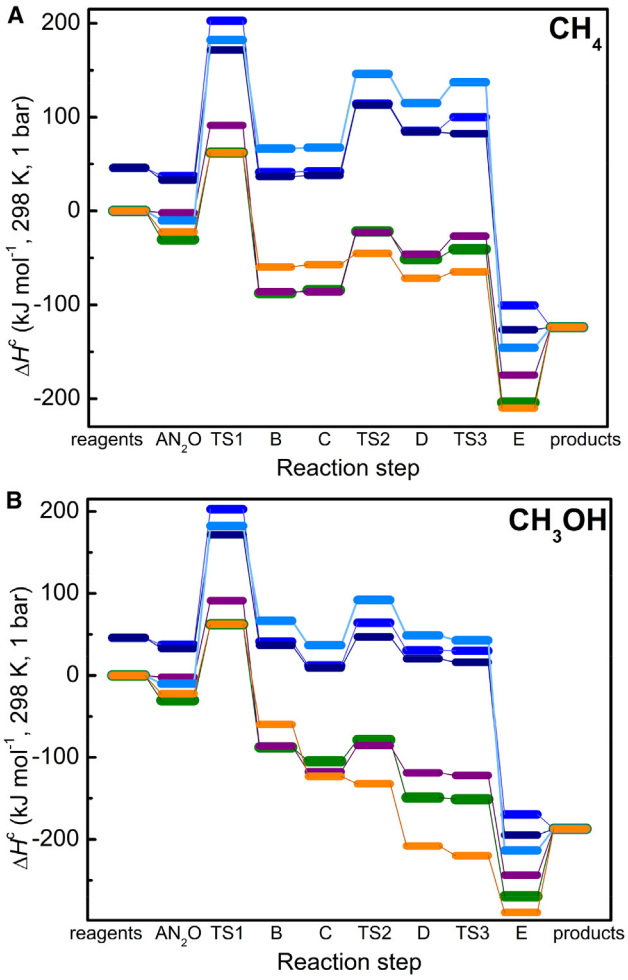

Figure 2. Methane-to-methanol and methanol-to-methylene glycol oxidation catalyzed on single-site iron catalysts

Reaction enthalpies for the oxidation of (A) methane to methanol and of (B) methanol to methylene glycol as computed at the UM06-L/def2-TZVP level following the cycle reported in Scheme 1 on the quintet spin energy surface for TauD (purple), Fe-BEA (orange), and Fe-MIL (green). For P450, the doublet (black), quartet (blue), and sextet (light blue) spin energy surfaces are reported. Enthalpies of the separated reactants in their ground state are taken as zero of the enthalpies (data in Tables S12–S24; see also Figures S4 and S5).

reasons, for P450, the reaction was followed on the doublet, quartet, and sextet spin surfaces.

Cartesian coordinates of all the structures optimized at the M06-L/def2-TZVP level are reported in xyz format in Data S1 (*.ZIP file). All relevant energetic parameters are reported in Tables S12–S24. The reaction enthalpies and the reaction Gibbs free energies provide an equivalent description of the reactivity of the clusters. The reaction profiles are discussed in the following in terms of reaction enthalpies in order to allow a direct comparison with literature data.[29,34,35,44,63] These profiles are shown in Figures 2A and 2B for the methane and the methanol cycle, respectively.

Formation of Fe(IV)=O and N_2O decomposition

The AN_2O → B reaction corresponds to adsorption of N_2O on the iron center and then to its decomposition to N_2 with the formation of the oxo species (B) through

Please cite this article in press as: Vitillo et al., Comparing the reaction profiles of single iron catalytic sites in enzymes and in reticular frameworks for methane-to-methanol oxidation, Cell Reports Physical Science (2023), https://doi.org/10.1016/j.xcrp.2023.101422

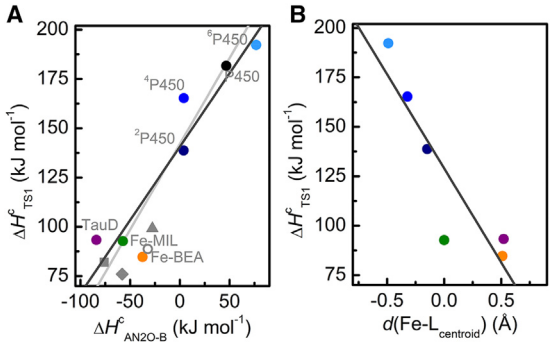

Figure 3. Descriptors for the N_2O decomposition reaction

(A) Reaction enthalpy for **AN_2O → B**, $\Delta H_{AN2O \rightarrow B}$, vs. the activation enthalpy, ΔH^c_{TS1}. Best linear fit is shown as dark gray solid line. The linear fit obtained in Vitillo et al.[35] on tri-metal oxo-centered clusters with different metal composition is also reported as a light gray line. Literature values reported for Fe-BEA[64] (empty circles), $Fe_{0.1}Mg_{1.9}(dobdc)_2$[34] (brown square), Fe-BTC[63] (yellow triangle), and Fe-BTT[44] (pink diamond), are also shown.

(B) The distance of iron from the centroid of two facing equatorial L in **A** d(Fe-L$_{centroid}$) vs. the activation enthalpy, ΔH^c_{TS1}. Negative and positive values of d(Fe-L$_{centroid}$) indicate, respectively, that the iron lies below or above the plane of the equatorial ligands with respect to the position that will be occupied by the oxo species in **AB**. Best linear fit is shown as a dark gray solid line. All the values have been obtained at the UM06-L/def2-TZVP level.

the transition state **TS1** (see Table S3). This is the rate-determining step of the reaction for all catalysts considered here. The reaction enthalpy $\Delta H_{AN2O \rightarrow B}$ for all the catalysts is reported in Figure 3A as a function of the activation enthalpy, ΔH^c_{TS1}. The reaction is exothermic for the non-heme catalysts, with the lowest $\Delta H_{AN2O \rightarrow B}$ value obtained for TauD (−83.9 kJ mol^{-1}) < Fe-MIL (−57.3 kJ mol^{-1}) < Fe-BEA (−37.5 kJ mol^{-1}). Bols et al. computed a similar value for iron-based zeolites (−32 kJ mol^{-1}).[64] For TauD and P450, notwithstanding the large body of literature on these enzymes, this reaction has not been modeled yet because N_2O is not the oxygen source commonly used for these systems. While the calculations indicate that N_2O can be a potential good oxidizer for **A-TauD**, for P450, the reaction is predicted to be almost isoenergetic for the doublet and the quartet and to be endothermic of 76.7 kJ mol^{-1} for the sextet. The ground spin state for P450 is predicted to change along this reaction from sextet (for **AN_2O**) to doublet (in **TS1** and **B**). This result agrees with the literature on P450 that indicates that the ground states for **A** and **AB** are the sextet and the doublet, respectively.[9,39] For **TS1**, the doublet and the sextet differ by only 10 kJ mol^{-1}, while this difference increases to 30 kJ mol^{-1} in **B**. The quartet spin state of **B** is only 5 kJ mol^{-1} higher in energy than the doublet, and it remains almost isoenergetic to it during the reaction up to **D**.

The computed ΔH^c_{TS1} values are all close to 90 kJ mol^{-1} for the non-heme catalysts, while P450 ΔH^c_{TS1} is significantly larger and shows a steep increase with higher spin: 139 kJ mol^{-1} for the doublet, 166 kJ mol^{-1} for the quartet, and 192 kJ mol^{-1} for the sextet. Considering the ground states along the reaction profile, ΔH^c_{TS1} for P450 is about double that obtained for the other catalysts (182 kJ mol^{-1}).

Previous studies indicated a Brønsted-Evans-Polanyi behavior for the N_2O dissociation reaction on single Fe species.[14,35,65,66] We verify that this is valid also for the catalysts considered here. The fitting line obtained (r^2 = 0.84; see dark gray line in Figure 3A) is very close to the one we obtained for single Fe(II) species in metal nodes of MIL-100 having different metal compositions (light gray line in Figure 3A).[35] Restricting the linear fit on P450 (min), Fe-MIL, TauD, and Fe-BEA results in a linear fit

coincident with the one obtained in Vitillo et al.,[35] suggesting once more the generality of the Brønsted-Evans-Polanyi (BEP) relationship for single iron-based systems.[14,35,65,66] Gani and Kulik[65] verified that the metal-ligand plane dihedral angle can also play a role in such a correlation. We have then studied the dependence of ΔH^{c}_{TS1} on geometric descriptors as the metal-ligand plane torsional angle (Fe-L-L-L, where L is an equatorial ligand; see Figure S1A), the distance of Fe from the axial donor *trans* to the oxo in **A** (see Figure S1B), and the distance of iron from the centroid of two opposite equatorial L in **A** (d(Fe-$L_{centroid}$); see Figure 3B). An inverse dependence was evidenced for the first two quantities, although with $r^2 \ll 0.5$, while a linear dependence was obtained for d(Fe-$L_{centroid}$) (r^2 = 0.77; solid line in Figure 3B). It is noteworthy that d(Fe-$L_{centroid}$) is negative only for P450 (see also Table S1); that is, the iron lies below the porphyrin plane. This is at the origin of the lower exothermicity of the coordination of N_2O (as verified by the lower N_2O adsorption enthalpies than for the non-heme catalysts) and of the reaction with it. **AB** species are instead all characterized by a positive d(Fe-$L_{centroid}$) (i.e., the iron is above the plane of its first ligands).

It has previously been noted[17,65] that the Fe=O bond is shorter and stronger in the absence of a ligand *trans* to the oxo. This is associated with the larger stabilization of the Fe $3d_z^2$ in a square pyramidal geometry compared with an octahedral one. Among the catalysts considered, Fe-BEA is the only **AB** species where the Fe is 5 coordinated and not 6 coordinated. Accordingly, **AB**-Fe-BEA shows the shortest Fe=O bond (1.606 Å; see Table S2).

The spin ladder obtained using DFT for **AB** species was assessed by multiconfiguration wave function-based methods for TauD, Fe-MIL, and Fe-BEA, while for P450, we have exploited the large literature on the multireference modeling of **AB-P450**.[9,54,55,59,61,62] The CASSCF/CASPT2 calculations for TauD, Fe-MIL, and Fe-BEA reached convergence only upon the inclusion in the active space of all the orbitals listed in Note S11: in particular, besides the 3*d* iron orbitals, the addition of the three doubly occupied 2*p* orbitals of the oxoferryl is mandatory (see Tables S25–S29). This corresponds to a (12,14) active space. Further increase in the active space to (14,15) did not result in a change in the spin ladders, confirming that convergence was achieved with (12,14).

The multireference calculations confirm the relative stability of the different spin states obtained by M06-L. They also agree with DFT in the description of the oxidation state of Fe in **AB** species. These results are summarized and discussed in Note S11.

C–H bond scission in methane and methanol

After the formation of the ferryl, N_2 is desorbed, and CH_4 is coordinated by the cluster (**C** intermediate). The reaction proceeds with the scission of the C–H bond with the formation of the **D** intermediate through the transition state **TS2**. For the reaction with methane, ΔH^{c}_{TS2} values were all found to be between 62 (Fe-MIL) and 78 kJ mol^{-1} (^{6}P450) except for Fe-BEA, which is characterized by a significantly lower value (12 kJ mol^{-1}; Figure 4A). A similar trend was observed for $\Delta H_{C \rightarrow D}$, with all the values found between 33 (Fe-MIL) and 48 kJ mol^{-1} (^{6}P450) while Fe-BEA lies well below (−14 kJ mol^{-1}). Fe-BEA is the only case where methane C–H bond scission is exothermic. ΔE^{c}_{TS2} values obtained in Oligaro et al.[37] for P450 at the B3LYP level with a double-ζ basis set (114.8 and 115.8 kJ mol^{-1} for the doublet and the quartet, respectively)[37] are close to the values obtained here (~95 kJ mol^{-1}; see Tables S12–S17), while $\Delta E^{c}_{C \rightarrow D}$ values (100 and 102.7 kJ mol^{-1} for the doublet and the quartet, respectively) are instead >50% larger than those calculated here (~55 kJ

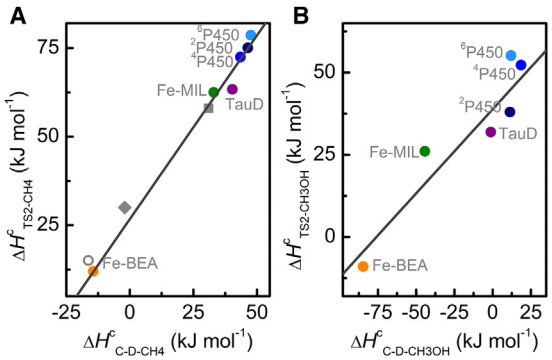

Figure 4. Brønsted-Evans-Polanyi behavior for C–H bond scission in methane and methanol

Reaction enthalpy for **C** → **D**, $\Delta H_{C \rightarrow D}$ vs. the activation enthalpy, ΔH^c_{TS2}, (A) for the methane and (B) for the methanol cycles as in Scheme 1. In (A), literature values reported for $Fe_{0.1}Mg_{1.9}(dobdc)_2$[34] (square), Fe-BTT[44] (diamond), and Fe-BEA[17] (empty circle) are also shown. The linear fit for methane (A, r^2 = 0.99) and methanol (B, r^2 = 0.83) data are reported as dark gray lines. All the values have been obtained at the UM06-L/def2-TZVP level.

mol^{-1}; see Tables S12–S17). For Fe-BEA, ΔH^c_{TS2} and $\Delta H_{C \rightarrow D}$ values are in quantitative agreement with the values obtained by Snyder et al.[17] using B3LYP and 6-311G* on Fe (15 and −16 kJ mol^{-1}, respectively).

The corresponding $\Delta H^c_{TS2-CH3OH}$ and $\Delta H_{C \rightarrow D\text{-}CH3OH}$ values obtained for the C–H activation of methanol qualitatively mirror the trends for C–H activation in methane, as evident from a comparison of Figures 4A and 4B. Moreover, BEP behavior is observed for the C–H scission step for both methane (Figure 4A) and methanol (Figure 4B) cycles.

ΔH^c_{TS2} values for methane and methanol are linearly correlated (r^2 = 0.88; Figure 5B). A similar dependence was also obtained for $\Delta H_{C \rightarrow D}$. Similar trends have been highlighted by Latimer et al.[5] for a larger set of catalysts. ΔH^c_{TS2} and $\Delta H_{C \rightarrow D}$ values for methanol are 30 and 40 kJ mol^{-1} smaller, respectively, than the corresponding values for methane. This agrees with the difference between the C–H bond dissociation enthalpy in methane and methanol (37 kJ mol^{-1}).[6] As a result, for Fe-BEA, the C–H bond scission in methanol is essentially barrierless if thermal contributions are considered (see Table S5).

Prior reports on catalysts for aliphatic C–H bond scission have evidenced a linear relationship between the activation energy for C–H bond cleavage (i.e., the **C** → **D** reaction energy)[65] and the reaction energy for formation of the oxo species.[14,67,68] This relationship holds also for the systems considered here, with Fe-BEA as an outlier in the ΔH^c_{TS2} vs. $\Delta H_{AN2O \rightarrow B}$ plot (Figure 5A). Deviations from this relationship have been associated with the presence of non-covalent interactions[14,65] or with distortions of the iron site.[65] Catalysts are in fact expected to lie on parallel lines in a ΔH^c_{TS2} vs. $\Delta H_{AN2O \rightarrow B}$ plot if the dihedral angle formed by the iron and its equatorial ligands (θ(Fe-L-L-L)) is significantly different.[65] **AB-Fe-BEA** is characterized by a significantly larger θ(Fe-L-L-L) in reference to the other catalysts considered (see Table S2). Moreover, this is the only catalyst where a *trans* ligand is missing. Fe-BTT,[44] where the *trans* ligand is located significantly far from the iron (~2 Å), is also an outlier of this plot (see Figure 5A). Five-coordinated ferryl species should then be preferred over six-coordinated ferryl species in order to design more reactive catalysts for the C–H bond scission in methane.

Other common descriptors used for ΔH^c_{TS2} are the ferryl bond length, d(Fe-O_{oxo}),[17] and the **AB** hydrogen affinity (E_H).[14,69] Although shorter d(Fe-O_{oxo}) and lower E_H

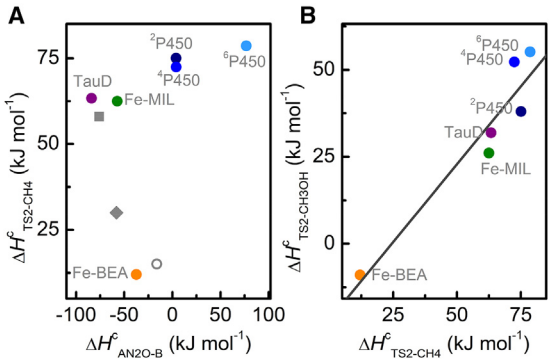

Figure 5. Descriptors for the C–H bond cleavage reaction in methane and methanol

(A) Activation enthalpy for **C** → **D**, ΔH^c_{TS2}, vs. the reaction enthalpy for $\mathbf{AN_2O}$ → **B**, $\Delta H_{AN2O \rightarrow B}$, for the methane cycle as in Scheme 1 for TauD, Fe-BEA, Fe-MIL, and P450. Literature values reported for $Fe_{0.1}Mg_{1.9}(dobdc)_2$[34] (square), Fe-BTC[63] (yellow triangle), Fe-BTT[44] (diamond), and Fe-BEA[17] (empty circle) are also shown.

(B) Activation enthalpy for **C** → **D** for methanol, $\Delta H^c_{TS2-CH3OH}$, vs. activation enthalpy for methane, $\Delta H^c_{TS2-CH4}$. The linear fit (r^2 = 0.88) is reported as a dark gray line. Values obtained at the UM06-L/def2-TZVP level.

correspond often to smaller ΔH^c_{TS2}, these relationships are not strictly valid for this group of catalysts (see Tables S2, S4, and S5 and Figure S2).

Radical rebound

The methyl (or the hydroxymethyl) radical in **D** reacts with the hydroxo species, resulting in the formation of methanol (methylene glycol) and the reduction of iron to its pristine oxidation state (**E**) through the transition state **TS3**.

The stability of **D** can be estimated through the enthalpy of adsorption of the alkyl radical. The enthalpy of adsorption decreases significantly going from methyl (−42 to −9 kJ mol^{-1}; see Table S6) to the hydroxymethyl radical (−121 to −37 kJ mol^{-1}; see Table S7). The larger stability of the hydroxymethyl complexes is due to the ability of the radical to engage the first-shell ligands of iron in hydrogen bonds using the –OH group, absent in the methyl radical. The largest increase in the adsorption enthalpy is observed for Fe-BEA (−25 and −121 kJ mol^{-1} for $CH_3\cdot$ and $(OH)CH_2\cdot$, respectively).

The activation enthalpies for this reaction step, ΔH^c_{TS3}, are all below 22 kJ mol^{-1} for methane (see Table S8), which is much lower than the corresponding ΔH^c_{TS1} and ΔH^c_{TS2} values. For methanol, it was not possible to locate a proper transition state because the rebound of the hydroxymethyl radical with the hydroxo species is essentially a barrierless process (see Table S9).

Catalyst regeneration

This step corresponds to the desorption of the product from the catalytic center. The quantity that better describes this step is the alcohol desorption enthalpy (see Figure S3 and Table S10 for **E-CH$_4$**, $-\Delta H^c_{CH3OH}$, and Table S11 for **E-CH$_3$OH**, $-\Delta H^c_{CH2(OH)2}$). The desorption enthalpies are only a few kJ mol^{-1} smaller for **E-CH$_4$** than for **E-CH$_3$OH**, and they follow the same trend: ^{6}P450 (31.9 and 37.7 kJ mol^{-1}, respectively) ∼^{4}P450 < ^{2}P450 < TauD < Fe-MIL < Fe-BEA (99.7 and 117.8 kJ mol^{-1}, respectively). The very low values of $-\Delta H^c_{CH3OH}$ and $-\Delta H^c_{CH2(OH)2}$ obtained for ^{6}P450 and ^{4}P450 are due to the same causes discussed for their small N_2O binding energy, i.e., the iron lies below the plane of its first shell ligands, making its

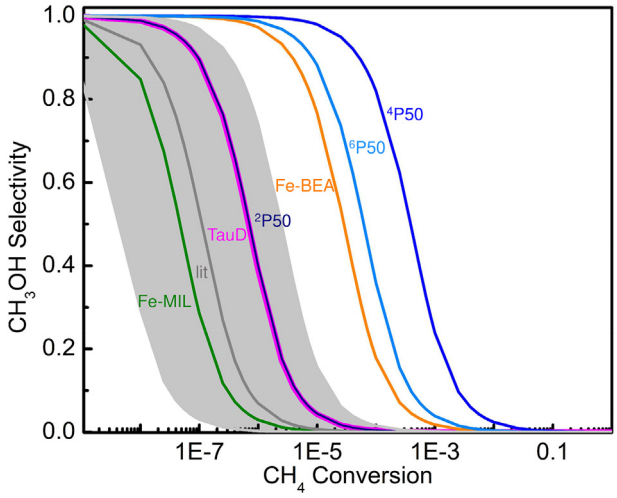

Figure 6. Methanol selectivity of single-site iron catalysts at ambient temperature

The selectivity is reported as function of the methane conversion at 25°C using Equations 2 and 3 for (from left to right) Fe-MIL (green), general curve (from Latimer et al.,[5] gray), TauD (magenta) ≅ ^{2}P450 (dark blue), Fe-BEA (orange), ^{6}P450 (light blue), and ^{4}P450 (blue). The gray curve was obtained in Latimer et al.[5] by regression of data obtained by modeling a large and diversified set of catalysts for methane and methanol reaction ($\pm 1\ \sigma$ error of this curve is indicated as gray areas).

interaction less effective with the alcohols. This makes alcohol desorption from **E-P450** and regeneration of P450 particularly favorable.

Methanol selectivity and rate constant

We have evaluated the methanol selectivity (S_{CH3OH}) of each catalyst using the definition adopted by Latimer et al.[5] Accordingly, a more selective catalyst is obtained by reducing the difference between the activation energy of the C–H bond scission for methane and methanol. In an ideal case, $\Delta G^{c}_{TS2-CH3OH}$ would be equal to or larger than $\Delta G^{c}_{TS2-CH4}$.

Figure 6 shows S_{CH3OH} as a function of methane conversion for the four catalysts at 25°C. The general relationship obtained in Latimer et al.[5] by reviewing a large number of different catalysts is also shown as a gray line, as extrapolated at 25°C. The shaded gray areas correspond to the $\pm 1\sigma$ error of this relationship ($\pm$7.7 kJ mol^{-1}). The standard deviation in experimental and theoretical ΔG^{c}_{TS2} values has been estimated to be about 10 kJ mol^{-1}.[5] This means that each curve reported in Figure 6 has an error comparable to the shaded areas.

Figure 6 demonstrates that the intrinsic selectivity of all the catalysts considered here is almost zero at ambient temperature for methane conversion >0.5%. This plot confirms once again that protection mechanisms are vital for keeping a low degree of methane overoxidation.[5,53] This concept was qualitatively explained for enzymes,[2] but now it is quantified for the first time. For lower methane conversions, ^{4}P450 is predicted to be the most selective, followed in order by ^{6}P450, Fe-BEA, TauD~^{2}P450, and Fe-MIL. It is noteworthy that the curves for the catalysts showing the largest displacement between Fe and the axial ligand in **C**, ^{4}P450 (2.5 Å), ^{6}P450 (2.5 Å), and Fe-BEA (∞), are well outside the shaded gray areas in Figure 6 on the right side of the plot, corresponding to higher methane selectivity. This indicates that the local structures around iron in ^{4}P450, ^{6}P450, and Fe-BEA make these catalysts intrinsically more selective than most catalysts reported in the literature. More

Please cite this article in press as: Vitillo et al., Comparing the reaction profiles of single iron catalytic sites in enzymes and in reticular frameworks for methane-to-methanol oxidation, Cell Reports Physical Science (2023), https://doi.org/10.1016/j.xcrp.2023.101422

explicitly, the methanol selectivity of ferryl species is larger when the trans ligand is weakly coordinating the iron or is absent (five-coordinated iron).

Direct MTM conversion in Fe-MIL has been reported in two recent studies[7,70] that highlighted the low levels of produced CO and CO_2. Simons et al.[7] experimentally proved that the high selectivity of Fe-MIL is associated with the formation of methoxy species that prevent the further oxidation of methanol. Accordingly, the green curve in Figure 6 points out that the active site of the MOF has the lowest intrinsic selectivity for the reaction among the catalysts considered here and most catalysts reported in the literature: in the absence of protection mechanisms, methane would be fully oxidized.

S_{CH3OH} dependence on T and the methane conversion makes the values of S_{CH3OH} significantly change upon modification of these two parameters. As an example, ^{4}P450 shows a S_{CH3OH} ~0 at room temperature (RT) at 1% methane conversion, while S_{CH3OH} increases to 0.2 at 120°C and is 0.12 at 10% methanol conversion at 300°C (curves not shown). These results show that caution is required in reviewing the methanol selectivity of a set of catalysts if the values are obtained at a different methane conversion and/or temperature.

The reaction rates for each catalyst (r_{cat}) have been calculated using Equation 1, where they are normalized to the Fe-MIL reaction. While Fe-BEA would have a reaction rate 3.3× that of Fe-MIL, the enzymes would be decidedly slower: TauD would have an r_{cat} of 0.12×, while $2 \cdot 10^{-10}$×, $1 \cdot 10^{-15}$×, and $2 \cdot 10^{-19}$× are predicted for ^{2}P450, ^{4}P450, and ^{6}P450, respectively. These very small r_{cat} values are due to the very large activation enthalpy necessary to dissociate N_2O by P450. N_2O would be not a suitable oxygen source for synthetic catalysts mimicking the P450 active site.

MTM catalyst design

We have evaluated the reactivity and selectivity of the catalytic site of two biomimetic models based on two enzymes (P450 and TauD) and two reticular frameworks catalysts (Fe-MIL and Fe-BEA) for the MTM reaction, using N_2O as oxygen source. The models were restricted to the first coordination shell of the iron center, allowing us to relate the local structure to the selectivity among the catalysts.

P450 and TauD models are often indicated among the target materials for selectivity and reactivity in the synthesis of bioinspired catalysts for C–H bond scission. Instead, calculations show that when restricting the models to the first coordination shell of iron, Fe-BEA has a lower activation barrier for C–H bond cleavage than MOFs and enzymes. This is an important result, placing the Fe-BEA zeolite as the most active catalyst, even more active than enzymes.

The highest enthalpic barrier for C–H bond scission (ΔH^c_{TS2}) is obtained for P450. This result points out that an active site mimicking a P450 active site in a synthetic supramolecular assembly (e.g., by introduction in a large surface area material as encapsulated guest species[71,72] or as part of the structure[73]) is not desirable. Moreover, based on the computed ΔH^c_{TS1}, N_2O would not constitute a suitable oxygen source for P450-inspired materials. This is an important point since N_2O is frequently used as an oxygen source in testing single iron heterogeneous catalysts. Substitution of the thiolate cysteinate ligand in P450 is a very effective tool to increase the enzyme catalytic activity toward very different reactions.[74,75] Selenocysteine-ligated P450s have, for example, shown higher rates for C–H bond cleavage than thiolate

cysteinate P450.[75] Metal substitution has been predicted to be another effective way to lower both ΔH^{c}_{TS1} and ΔH^{c}_{TS2}.[76]

On the other hand, the ΔH^{c}_{TS1} and ΔH^{c}_{TS2} values for TauD are similar to those for Fe-MIL, while the intrinsic selectivity of the local structure around iron is higher, making TauD and its experimental biomimetic model interesting for inspiring new heterogeneous catalysts.

Although as an average, this first coordination shell approach in designing new catalysts based on reticular frameworks can give positive results in the context of thermodynamics, this is not true if we consider selectivity. In fact, all the models show selectivity close to zero for methane conversions exceeding 1% at ambient temperature. It is then evident that the design of selective catalysts for MTM requires going beyond those just involving perturbations of the first coordination shell of iron. Protective mechanisms[5,7] and appropriate microenvironment design[2,5,53] are mandatory for selective oxidation of MTM for all these catalysts. The efficacy of protection mechanisms in improving methanol selectivity has been proven experimentally by Simons et al.[7] for the catalyst having the lowest intrinsic selectivity in our study: for Fe-MIL, the selectivity at 120°C was kept up to 73% for methane conversion of about 30% by mixing the MOF with an acidic zeolite, which serves to protect methanol by dehydration, and storing the methoxy species formed, which can be recovered by exposing the catalyst to water. Very recently, Fujisaki et al.[8] have reported that extending the design of an N-heterocyclic carbene-ligated Fe(II) complex beyond the chemically coordinated ligands can significantly improve the selectivity of MTM. They have verified that increasing the size of hydrophobic ligands around the iron center can increase methanol selectivity from 35% to 83%. This high selectivity was achieved because the homogeneous catalyst was tested in aqueous solution, which acts as a storage medium of the hydrophilic methanol product. Ligands in MOFs are often hydrophobic. Tri-iron oxo-centered MOFs with phenyl[50] and biphenyl ligands[77,78] have been reported. In their paper, Simons et al.[7] verified an increase in the methanol selectivity upon increasing the linker dimension from phenyl to biphenyl, confirming the validity of the strategy in Fujisaki et al.[8] also for the reaction in the gas phase. Nevertheless, a selectivity comparable to the one obtained for the reaction in aqueous medium by Fujisaki et al.[8] was obtained only when the reticular framework catalysts were mixed with an amount of hydrophilic protecting medium (an acidic zeolite) in quantities >10× that of the MOF in terms of formula units.[7]

Although the selectivity is very low, it is noteworthy that Fe-BEA and P450 active sites are shown to be intrinsically more selective than the most part of the catalysts studied so far[5] for the MTM reaction. Fe-BEA shows ΔH^{c}_{TS1} and ΔH^{c}_{TS2} values that are not only the lowest among the catalysts considered here but that are very low also in absolute terms (values in agreement with previous calculations and experimental observation).[17,31] Based on the results obtained here, for maintaining high methanol selectivity, the design of the reaction microenvironment and the introduction of protection mechanisms are essential, and five-coordinated ferryl species are predicted to reach larger yield and rates in comparison with six-coordinated species.

EXPERIMENTAL PROCEDURES

Resource availability

Lead contact

Further information and requests for resources should be directed to and will be fulfilled by the lead contact, Jenny G. Vitillo (jg.vitillo@gmail.com).

Materials availability

No new materials were generated in this study.

Data and code availability

Cartesian coordinates of all the structures discussed in the article are reported in xyz format in Data S1 (*.ZIP file). They are also available at the Zenodo repository with https://doi.org/10.5281/zenodo.6632726.

Density functional calculations

All KS-DFT calculations were performed using the *Gaussian 16* program.[79] M06-L[80] density functional in its unrestricted formalism (U) was used in combination with the def2-TZVP basis sets.[81,82] This level of theory has been shown to give similar results of multireference wave function calculations for Fe-based catalysts.[34,35,83] Moreover, we have verified in a coupled experimental-computational study that it predicts correctly the experimental activation energy for N_2O decomposition on MIL-100(Fe).[29]

P450 was simulated using the Cpd I model reported in Oligaro et al.[37] where the functional groups of the porphyrin ring are substituted with hydrogen atoms and the full cysteinato ligand is replaced by the shorter SH^- (see first column in Figure 1), allowing a better modeling of the enzyme.[37]

A homogeneous model of the catalytic site of TauD active form (TauD-*J*) has been recently synthetized by Biswas et al.:[38] $[Fe(IV)O(TQA)(CH_3CN)]^{2+}$ (TQA = tris(2-quinolylmethyl)amine). Although the first-shell ligands of iron are different than in TauD (TQA and CH_3CN vs. two histidine, KG, aspartic acid),[84] the authors showed that this compound is able to reproduce both the functional and the electronic properties of TauD-*J*. In particular, it is able to oxidize both C−H and C=C bonds at −40°C.[38] We have then adopted $[Fe(IV)O(TQA)(CH_3CN)]^{2+}$ as the model for the catalytic active form of TauD (see second column in Figure 1) and derived its reduced forms using the cycle in Scheme 1.

α-Fe in *BEA zeolite has been simulated using the model adopted by Snyder et al.[17] to study the C–H bond activation of methane on this catalyst. This model (Fe-BEA, in the following) is shown in the third column of Figure 1. This cluster has been successfully used to simulate the catalytic conversion of MTM by α-Fe sites and played a crucial role in the identification of the structure of α-Fe through spectroscopic techniques.[17] In order to include the structural constraints of the zeolite framework, particularly important for this system, only the positions of the adsorbates, the iron center, and the first and second coordination shells have been optimized.[17]

The cluster used for the tri-iron oxo-centered metal nodes of MIL-100(Fe) is reported in the fourth column of Figure 1 (Fe-MIL, in the following). In order to make it a single iron center, the tri-valent irons have been substituted by Al^{+3}.[14] Formates are used to saturate the cluster (formula: $Al_2Fe(II)(\mu_3\text{-}O)(COO)_6$).[29,35,85] This cluster has been shown to provide results fully comparable with larger clusters saturated with benzoates (see Note S12 and Figure S19).[14,85] Moreover, this model is able to reproduce the experimental activation energy for N_2O decomposition on MIL-100(Fe)[29] and the experimental infrared (IR) vibrational shift of CO and NO at different coverages on tri-iron oxo-centered MOFs.[86]

Geometry optimization was carried out by means of the Berny optimization algorithm with analytical gradient and default convergence thresholds. A (99,590)

pruned grid was used (i.e., 99 radial points and 590 angular points per radial point), corresponding to the grid = ultrafine option. All the energetic data have been corrected for the basis set superposition error (BSSE) following the *a posteriori* method proposed by Boys and Bernardi[87] as implemented in *Gaussian 16*. The BSSE-corrected energetic values are indicated by a c superscript and were obtained from the computed Y values as $Y^c = Y + \mathrm{BSSE}$.

Unscaled, harmonic vibrational frequencies were computed analytically. Enthalpies and Gibbs free energies were calculated at 1 atm and 298 K from conventional ideal gas, rigid rotator, particle in a box, and quantum mechanical harmonic oscillator partition functions, except that low vibrational frequencies (<50 cm^{-1}) replaced by a cutoff value (50 cm^{-1}) account for limitations in the harmonic oscillator approximation for very-low-frequency vibrations.[88–92] Charge and spin densities were obtained using Charge Model 5 (CM5)[93] and Hirshfeld population analysis,[94] respectively. Spin densities are expressed as the difference between the α and β electron densities.

The reaction rate of each catalyst normalized (r_{cat}) with respect to that of Fe-MIL is estimated using the formula[38]

$$r_{cat} = \frac{k_{cat}}{k_{Fe-MIL}} = e^{\left(\Delta G^{act}_{Fe-MIL} - \Delta G^{act}_{cat}\right)/(RT)}, \qquad \text{(Equation 1)}$$

where R is the molar gas constant (in J mol^{-1} K^{-1}), T is a reference temperature (in K, 298 K in this study), ΔG^{act}_{cat} is the Gibbs free energy associated with the rate-determining step for the catalyst (in J mol^{-1}), and ΔG^{act}_{Fe-MIL} is the Gibbs free energy associated with the rate-determining step for Fe-MIL (in J mol^{-1}).

The selectivity of the catalyst for methanol (S_{CH3OH}) was evaluated using the formula derived by Latimer et al.[5] for radical-like C–H bond activation by single-site catalysts in a continuous catalytic process:

$$S_{CH3OH} = \frac{1 - X - (1 - X)^{k_2/k_1}}{X[(k_2/k_1) - 1]}, \qquad \text{(Equation 2)}$$

where X is the methane conversion and k_1 and k_2 are the rate constants for the $CH_4 \rightarrow CH_3OH$ and $CH_3OH \rightarrow CO_2$ reactions, respectively. $\frac{k_2}{k_1}$ is defined as

$$\frac{k_2}{k_1} = e^{\frac{\Delta G_{TS2,CH4} - \Delta G_{TS2,CH3OH}}{RT}}, \qquad \text{(Equation 3)}$$

where T is 298 K and $\Delta G_{TS2,CH4}$ and $\Delta G_{TS2,CH3OH}$ are the Gibbs free energy associated with the C–H bond activation step in Scheme 1 for methane and methanol, respectively (in J mol^{-1}). This expression of S_{CH3OH} approximates the real selectivity, assuming that each reacted methane would be converted to methanol, and it is used only for the sake of comparison.[5] In real systems, protection mechanisms and other oxidation reactions can take place that can increase or decrease the selectivity with respect to S_{CH3OH}.[5,7] Neglecting overoxidation reactions that are not originating from methanol is a very mild approximation. As an example, surface methoxy species can be formed in significant amounts during the MTM reaction in zeolites and MOFs.[7,30] Nevertheless, methoxy species act in these systems as stable intermediates that protect methanol from overoxidation. It is a matter of fact that the alcohols formed from the oxidation of simple alkanes cannot be recovered from zeolites and MOFs by thermal treatment, but this is only possible through water extraction.[7,17,28,29]

Multireference wave function calculations

Single-point calculations at the optimized DFT geometries on the structures as in Figure 1 of TauD, Fe-MIL, and Fe-BEA were performed using the complete active

space self-consistent field (CASSCF)[95] method followed by perturbation theory to second order (CASPT2)[96] as implemented in the Open Molcas 19.11 program.[97] Only for the Fe-BEA was the model adopted for multireference calculations obtained from that in Figure 1 by eliminating all the atoms outside the double 6MR unit and saturating the oxygen dangling bonds with H (see Figure S6). Relativistic all-electrons ANO-RCC basis sets were used for all the atoms,[98,99] triple-ζ quality for N, O, Al, and Fe atoms and double-ζ quality for Si, C and H. For Fe-BEA, the basis set quality was lowered to double-ζ quality for Al and O and to ANO-RCC-MB for all the H and for the atoms belonging to the six-member ring not containing the iron. The resolution of identity combined with the Cholesky decomposition was used to reduce the cost associated with the treatment of two-electron integrals. No symmetric constraints were imposed on the wavefunction. The active space was constructed including[34,54] all the molecular orbitals having the main contribution from (1) the five 3*d* orbitals of the Fe center, (2) the five correlating 3*d*′ orbitals of the Fe center, (3) the three doubly occupied 2*p* orbitals of the oxoferryl (O_{oxo}), and (4) one doubly occupied orbital to account for the covalent interaction of the Fe and the first neighbors. The active space included 12 electrons and 14 orbitals (12,14). A larger active space (14,15) was obtained by considering an additional doubly occupied orbital to check for the convergence of the active space for TauD, Fe-BEA, and Fe-MIL (see Note S10 and Figures S7–S18).

SUPPLEMENTAL INFORMATION

Supplemental information can be found online at https://doi.org/10.1016/j.xcrp.2023.101422.

ACKNOWLEDGMENTS

This work was partially supported by the Inorganometallic Catalyst Design Center; an Energy Frontier Research Center funded by the US Department of Energy, Office of Science, Basic Energy Sciences, under award no. DE-SC0012702; and by the Catalyst Design for Decarbonization Center, an Energy Frontier Research Center funded by the US Department of Energy, Office of Science, Basic Energy Sciences, under award no. DE-SC0023383. The authors acknowledge the Minnesota Supercomputing Institute (MSI) at the University of Minnesota for providing computational resources.

AUTHOR CONTRIBUTIONS

Conceptualization, J.G.V.; methodology, J.G.V.; investigation, J.G.V.; writing – original draft, J.G.V.; writing – review & editing, J.G.V., C.C.L., A.B., and L.G.; funding acquisition, L.G.; supervision, J.G.V.

DECLARATION OF INTERESTS

The authors declare no competing interests.

INCLUSION AND DIVERSITY

We support inclusive, diverse, and equitable conduct of research.

Received: February 20, 2023
Revised: April 23, 2023
Accepted: May 1, 2023
Published: May 22, 2023

REFERENCES

1. Hagen, J. (2006). Industrial Catalysis: A Practical Approach, Second edition (Wiley-VCH Verlag GmbH & Co. KGaA).
2. Snyder, B.E.R., Bols, M.L., Schoonheydt, R.A., Sels, B.F., and Solomon, E.I. (2018). Iron and copper active sites in zeolites and their correlation to metalloenzymes. Chem. Rev. *118*, 2718–2768. https://doi.org/10.1021/acs.chemrev.7b00344.
3. Vaissier Welborn, V., and Head-Gordon, T. (2019). Computational design of synthetic enzymes. Chem. Rev. *119*, 6613–6630. https://doi.org/10.1021/acs.chemrev.8b00399.
4. Ravi, M., Ranocchiari, M., and van Bokhoven, J.A. (2017). The direct catalytic oxidation of methane to methanol—a critical assessment. Angew. Chem. Int. Ed. *56*, 16464–16483. https://doi.org/10.1002/anie.201702550.
5. Latimer, A.A., Kakekhani, A., Kulkarni, A.R., and Nørskov, J.K. (2018). Direct methane to methanol: the selectivity–conversion limit and design strategies. ACS Catal. *8*, 6894–6907. https://doi.org/10.1021/acscatal.8b00220.
6. Blanksby, S.J., and Ellison, G.B. (2003). Bond dissociation energies of organic molecules. Acc. Chem. Res. *36*, 255–263. https://doi.org/10.1021/ar020230d.
7. Simons, M.C., Prinslow, S.D., Babucci, M., Hoffman, A.S., Hong, J., Vitillo, J.G., Bare, S.R., Gates, B.C., Lu, C.C., Gagliardi, L., and Bhan, A. (2021). Beyond radical rebound: methane oxidation to methanol catalyzed by iron species in metal–organic framework nodes. J. Am. Chem. Soc. *143*, 12165–12174. https://doi.org/10.1021/jacs.1c04766.
8. Fujisaki, H., Ishizuka, T., Kotani, H., Shiota, Y., Yoshizawa, K., and Kojima, T. (2023). Selective methane oxidation by molecular iron catalysts in aqueous medium. Nature *616*, 476–481. https://doi.org/10.1038/s41586-023-05821-2.
9. Shaik, S., Cohen, S., Wang, Y., Chen, H., Kumar, D., and Thiel, W. (2010). P450 enzymes: their structure, reactivity, and selectivity—modeled by QM/MM calculations. Chem. Rev. *110*, 949–1017. https://doi.org/10.1021/cr900121s.
10. Borovik, A.S. (2005). Bioinspired hydrogen bond motifs in ligand design: the role of noncovalent interactions in metal ion mediated activation of dioxygen. Acc. Chem. Res. *38*, 54–61. https://doi.org/10.1021/ar030160q.
11. de Visser, S.P., Ogliaro, F., Sharma, P.K., and Shaik, S. (2002). What factors affect the regioselectivity of oxidation by cytochrome P450? A DFT study of allylic hydroxylation and double bond epoxidation in a model reaction. J. Am. Chem. Soc. *124*, 11809–11826. https://doi.org/10.1021/ja026872d.
12. Shook, R.L., and Borovik, A.S. (2010). Role of the secondary coordination sphere in metal-mediated dioxygen activation. Inorg. Chem. *49*, 3646–3660. https://doi.org/10.1021/ic901550k.
13. Schyman, P., Lai, W., Chen, H., Wang, Y., and Shaik, S. (2011). The directive of the protein: how does cytochrome P450 select the mechanism of dopamine formation? J. Am. Chem. Soc. *133*, 7977–7984. https://doi.org/10.1021/ja201665x.
14. Vitillo, J.G., Lu, C.C., Cramer, C.J., Bhan, A., and Gagliardi, L. (2021). Influence of first and second coordination environment on structural Fe(II) sites in MIL-101 for C–H bond activation in methane. ACS Catal. *11*, 579–589. https://doi.org/10.1021/acscatal.0c03906.
15. Zilly, F.E., Acevedo, J.P., Augustyniak, W., Deege, A., Häusig, U.W., and Reetz, M.T. (2011). Tuning a P450 enzyme for methane oxidation. Angew. Chem. Int. Ed. *50*, 2720–2724. https://doi.org/10.1002/anie.201006587.
16. Gherman, B.F., Lippard, S.J., and Friesner, R.A. (2005). Substrate hydroxylation in methane monooxygenase: quantitative modeling via mixed quantum mechanics/molecular mechanics techniques. J. Am. Chem. Soc. *127*, 1025–1037. https://doi.org/10.1021/ja049847b.
17. Snyder, B.E.R., Vanelderen, P., Bols, M.L., Hallaert, S.D., Böttger, L.H., Ungur, L., Pierloot, K., Schoonheydt, R.A., Sels, B.F., and Solomon, E.I. (2016). The active site of low-temperature methane hydroxylation in iron-containing zeolites. Nature *536*, 317–321. https://doi.org/10.1038/nature19059.
18. Groves, J.T. (2003). The bioinorganic chemistry of iron in oxygenases and supramolecular assemblies. Proc. Natl. Acad. Sci. USA *100*, 3569–3574. https://doi.org/10.1073/pnas.0830019100.
19. Warshel, A. (1978). Energetics of enzyme catalysis. Proc. Natl. Acad. Sci. USA *75*, 5250–5254. https://doi.org/10.1073/pnas.75.11.5250.
20. Moliner, V. (2011). Eppur si muove" (yet it moves). Proc. Natl. Acad. Sci. USA *108*, 15013–15014. https://doi.org/10.1073/pnas.1112014108.
21. Adamczyk, A.J., Cao, J., Kamerlin, S.C.L., and Warshel, A. (2011). Catalysis by dihydrofolate reductase and other enzymes arises from electrostatic preorganization, not conformational motions. Proc. Natl. Acad. Sci. USA *108*, 14115–14120. https://doi.org/10.1073/pnas.1111252108.
22. Balcells, D., Clot, E., and Eisenstein, O. (2010). C—H bond activation in transition metal species from a computational perspective. Chem. Rev. *110*, 749–823. https://doi.org/10.1021/cr900315k.
23. Kumar, R., Pandey, B., Sen, A., Ansari, M., Sharma, S., and Rajaraman, G. (2020). Role of oxidation state, ferryl-oxygen, and ligand architecture on the reactivity of popular high-valent FeIV=O species: a theoretical perspective. Coord. Chem. Rev. *419*, 213397. https://doi.org/10.1016/j.ccr.2020.213397.
24. Sun, D., Ye, L., and Li, Z. (2015). Visible-light-assisted aerobic photocatalytic oxidation of amines to imines over NH2-MIL-125(Ti). Appl. Catal., B *164*, 428–432. https://doi.org/10.1016/j.apcatb.2014.09.054.
25. Bunting, R.J., Rice, P.S., Thompson, J., and Hu, P. (2021). Investigating the innate selectivity issues of methane to methanol: consideration of an aqueous environment. Chem. Sci. *12*, 4443–4449. https://doi.org/10.1039/D0SC05402J.
26. Warshel, A., and Weiss, R.M. (1980). An empirical valence bond approach for comparing reactions in solutions and in enzymes. J. Am. Chem. Soc. *102*, 6218–6226. https://doi.org/10.1021/ja00540a008.
27. Blankenship, A.N., Ravi, M., Newton, M.A., and van Bokhoven, J.A. (2021). Heterogeneously catalyzed aerobic oxidation of methane to a methyl derivative. Angew. Chem. Int. Ed. *60*, 18138–18143. https://doi.org/10.1002/anie.202104153.
28. Xiao, D.J., Bloch, E.D., Mason, J.A., Queen, W.L., Hudson, M.R., Planas, N., Borycz, J., Dzubak, A.L., Verma, P., Lee, K., et al. (2014). Oxidation of ethane to ethanol by N2O in a metal–organic framework with coordinatively unsaturated iron(II) sites. Nat. Chem. *6*, 590–595. https://doi.org/10.1038/nchem.1956.
29. Simons, M.C., Vitillo, J.G., Babucci, M., Hoffman, A.S., Boubnov, A., Beauvais, M.L., Chen, Z., Cramer, C.J., Chapman, K.W., Bare, S.R., et al. (2019). Structure, dynamics, and reactivity for light alkane oxidation of Fe(II) sites situated in the nodes of a metal–organic framework. J. Am. Chem. Soc. *141*, 18142–18151. https://doi.org/10.1021/jacs.9b08686.
30. Zecchina, A., Rivallan, M., Berlier, G., Lamberti, C., and Ricchiardi, G. (2007). Structure and nuclearity of active sites in Fe-zeolites: comparison with iron sites in enzymes and homogeneous catalysts. Phys. Chem. Chem. Phys. *9*, 3483–3499. https://doi.org/10.1039/B703445H.
31. Bols, M.L., Hallaert, S.D., Snyder, B.E.R., Devos, J., Plessers, D., Rhoda, H.M., Dusselier, M., Schoonheydt, R.A., Pierloot, K., Solomon, E.I., and Sels, B.F. (2018). Spectroscopic identification of the α-Fe/α-O active site in Fe-CHA zeolite for the low-temperature activation of the methane C-H bond. J. Am. Chem. Soc. *140*, 12021–12032. 10.1021/jacs.8b05877. https://doi.org/10.1021/jacs.1028b05877.
32. Kulik, H.J., Vennelakanti, V., Nandy, A., and Kulik, H. (2021). The effect of Hartree-Fock exchange on scaling relations and reaction energetics for C–H activation catalysts. Preprint at ChemRxiv. https://doi.org/10.26434/chemrxiv.14766531.v1.
33. Vogt, E.T.C., Whiting, G.T., Dutta Chowdhury, A., and Weckhuysen, B.M. (2015). Chapter two - zeolites and zeotypes for oil and gas conversion. In Advances in Catalysis, F.C. Jentoft, ed. (Academic Press), pp. 143–314. https://doi.org/10.1016/bs.acat.2015.10.001.
34. Verma, P., Vogiatzis, K.D., Planas, N., Borycz, J., Xiao, D.J., Long, J.R., Gagliardi, L., and Truhlar, D.G. (2015). Mechanism of oxidation of ethane to ethanol at iron(IV)–Oxo sites in magnesium-diluted Fe2(dobdc). J. Am. Chem. Soc. *137*, 5770–5781. https://doi.org/10.1021/jacs.5b00382.
35. Vitillo, J.G., Bhan, A., Cramer, C.J., Lu, C.C., and Gagliardi, L. (2019). Quantum chemical characterization of structural single Fe(II) sites in MIL-type metal–organic frameworks for the oxidation of methane to methanol and ethane

to ethanol. ACS Catal. *9*, 2870–2879. https://doi.org/10.1021/acscatal.8b04813.

36. Bollinger, J.M., Jr., Price, J.C., Hoffart, L.M., Barr, E.W., and Krebs, C. (2005). Mechanism of Taurine: α-ketoglutarate dioxygenase (TauD) from *Escherichia coli*. Eur. J. Inorg. Chem. *2005*, 4245–4254. https://doi.org/10.1002/ejic.200500476.

37. Ogliaro, F., Harris, N., Cohen, S., Filatov, M., de Visser, S.P., and Shaik, S. (2000). A model "rebound" mechanism of hydroxylation by cytochrome P450: stepwise and effectively concerted pathways, and their reactivity patterns. J. Am. Chem. Soc. *122*, 8977–8989. https://doi.org/10.1021/ja991878x.

38. Biswas, A.N., Puri, M., Meier, K.K., Oloo, W.N., Rohde, G.T., Bominaar, E.L., Münck, E., and Que, L. (2015). Modeling TauD-J: a high-spin nonheme oxoiron(IV) complex with high reactivity toward C–H bonds. J. Am. Chem. Soc. *137*, 2428–2431. https://doi.org/10.1021/ja511757j.

39. Shaik, S., Kumar, D., de Visser, S.P., Altun, A., and Thiel, W. (2005). Theoretical perspective on the structure and mechanism of cytochrome P450 enzymes. Chem. Rev. *105*, 2279–2328. https://doi.org/10.1021/cr030722j.

40. Caddell Haatveit, K., Garcia-Borràs, M., and Houk, K.N. (2018). Computational protocol to understand P450 mechanisms and design of efficient and selective biocatalysts. Front. Chem. *6*, 663. https://doi.org/10.3389/fchem.2018.00663.

41. Hausinger, R.P. (2004). Fe(II)/α-ketoglutarate-dependent hydroxylases and related enzymes. Crit. Rev. Biochem. Mol. Biol. *39*, 21–68. https://doi.org/10.1080/10409230490440541.

42. Price, J.C., Barr, E.W., Glass, T.E., Krebs, C., and Bollinger, J.M. (2003). Evidence for hydrogen abstraction from C1 of taurine by the high-spin Fe(IV) intermediate detected during oxygen activation by taurine:α-ketoglutarate dioxygenase (TauD). J. Am. Chem. Soc. *125*, 13008–13009. https://doi.org/10.1021/ja037400h.

43. Dinh, K.T., Sullivan, M.M., Serna, P., Meyer, R.J., Dincă, M., and Román-Leshkov, Y. (2018). Viewpoint on the partial oxidation of methane to methanol using Cu- and Fe-exchanged zeolites. ACS Catal. *8*, 8306–8313. https://doi.org/10.1021/acscatal.8b01180.

44. Vogiatzis, K.D., Haldoupis, E., Xiao, D.J., Long, J.R., Siepmann, J.I., and Gagliardi, L. (2016). Accelerated computational analysis of metal–organic frameworks for oxidation catalysis. J. Phys. Chem. C *120*, 18707–18712. https://doi.org/10.1021/acs.jpcc.6b07115.

45. Xiao, D.J., Oktawiec, J., Milner, P.J., and Long, J.R. (2016). Pore environment effects on catalytic cyclohexane oxidation in expanded Fe2(dobdc) analogues. J. Am. Chem. Soc. *138*, 14371–14379. https://doi.org/10.1021/jacs.6b08417.

46. Osadchii, D.Y., Olivos-Suarez, A.I., Szécsényi, Á., Li, G., Nasalevich, M.A., Dugulan, I.A., Crespo, P.S., Hensen, E.J.M., Veber, S.L., Fedin, M.V., et al. (2018). Isolated Fe sites in metal organic frameworks catalyze the direct conversion of methane to methanol. ACS Catal. *8*, 5542–5548. https://doi.org/10.1021/acscatal.8b00505.

47. Szécsényi, Á., Li, G., Gascon, J., and Pidko, E.A. (2018). Unraveling reaction networks behind the catalytic oxidation of methane with H2O2 over a mixed-metal MIL-53(Al,Fe) MOF catalyst. Chem. Sci. *9*, 6765–6773. https://doi.org/10.1039/C8SC02376J.

48. Rogge, S.M.J., Bavykina, A., Hajek, J., Garcia, H., Olivos-Suarez, A.I., Sepúlveda-Escribano, A., Vimont, A., Clet, G., Bazin, P., Kapteijn, F., et al. (2017). Metal-organic and covalent organic frameworks as single-site catalysts. Chem. Soc. Rev. *46*, 3134–3184. https://doi.org/10.1039/C7CS00033B.

49. Zhao, W., Shi, Y., Jiang, Y., Zhang, X., Long, C., An, P., Zhu, Y., Shao, S., Yan, Z., Li, G., and Tang, Z. (2021). Fe-O clusters anchored on nodes of metal–organic frameworks for direct methane oxidation. Angew. Chem. Int. Ed. *60*, 5811–5815. https://doi.org/10.1002/anie.202013807.

50. Horcajada, P., Surblé, S., Serre, C., Hong, D.-Y., Seo, Y.-K., Chang, J.-S., Grenèche, J.M., Margiolaki, I., and Férey, G. (2007). Synthesis and catalytic properties of MIL-100(Fe), an iron(iii) carboxylate with large pores. Chem. Commun. 2820–2822. https://doi.org/10.1039/B704325B.

51. Chevreau, H., Permyakova, A., Nouar, F., Fabry, P., Livage, C., Ragon, F., Garcia-Marquez, A., Devic, T., Steunou, N., Serre, C., and Horcajada, P. (2016). Synthesis of the biocompatible and highly stable MIL-127(Fe): from large scale synthesis to particle size control. CrystEngComm *18*, 4094–4101. https://doi.org/10.1039/C5CE01864A.

52. Macreadie, L.K., Babarao, R., Setter, C.J., Lee, S.J., Qazvini, O.T., Seeber, A.J., Tsanaktsidis, J., Telfer, S.G., Batten, S.R., and Hill, M.R. (2020). Enhancing multicomponent metal-organic frameworks for low pressure liquid organic hydrogen carrier separations. Angew. Chem. Int. Ed. *59*, 6090–6098. https://doi.org/10.1002/anie.201916159.

53. Snyder, B.E.R., Bols, M.L., Rhoda, H.M., Plessers, D., Schoonheydt, R.A., Sels, B.F., and Solomon, E.I. (2021). Cage effects control the mechanism of methane hydroxylation in zeolites. Science *373*, 327–331. https://doi.org/10.1126/science.abd5803.

54. Phung, Q.M., and Pierloot, K. (2019). Low-lying electromeric states in chloro-ligated iron(IV)-Oxo porphyrin as a model for compound I, studied with second-order perturbation theory based on density matrix renormalization group. J. Chem. Theor. Comput. *15*, 3033–3043. https://doi.org/10.1021/acs.jctc.9b00166.

55. Radoń, M., and Broclawik, E. (2019). Electronic properties of iron sites and their active forms in porphyrin-type architectures. In Computational Methods to Study the Structure and Dynamics of Biomolecules and Biomolecular Processes: From Bioinformatics to Molecular Quantum Mechanics, A. Liwo, ed. (Springer International Publishing), pp. 755–823. https://doi.org/10.1007/978-3-319-95843-9_23.

56. Rittle, J., and Green, M.T. (2010). Cytochrome P450 compound I: capture, characterization, and C-H bond activation kinetics. Science *330*, 933–937. https://doi.org/10.1126/science.1193478.

57. Phung, Q.M., Martín-Fernández, C., Harvey, J.N., and Feldt, M. (2019). Ab initio calculations for spin-gaps of non-heme iron complexes. J. Chem. Theor. Comput. *15*, 4297–4304. https://doi.org/10.1021/acs.jctc.9b00370.

58. Shaik, S., Munro, A.W., Sen, S., Mowat, C., Nam, W., Derat, E., Bugg, T., Proshlyakov, D.A., Hausinger, R.P., Straganz, G.D., et al. (2011). Iron-Containing Enzymes: Versatile Catalysts of Hydroxylation Reactions in Nature (Royal Society of Chemistry). https://doi.org/10.1039/9781849732987.

59. Radoń, M., and Broclawik, E. (2007). Peculiarities of the electronic structure of cytochrome P450 compound I: CASPT2 and DFT modeling. J. Chem. Theor. Comput. *3*, 728–734. https://doi.org/10.1021/ct600363a.

60. Vancoillie, S., Zhao, H., Radoń, M., and Pierloot, K. (2010). Performance of CASPT2 and DFT for relative spin-state energetics of heme models. J. Chem. Theor. Comput. *6*, 576–582. https://doi.org/10.1021/ct900567c.

61. Schöneboom, J.C., Neese, F., and Thiel, W. (2005). Toward identification of the compound I reactive intermediate in cytochrome P450 chemistry: a QM/MM study of its EPR and mössbauer parameters. J. Am. Chem. Soc. *127*, 5840–5853. https://doi.org/10.1021/ja0424732.

62. Altun, A., Shaik, S., and Thiel, W. (2007). What is the active species of cytochrome P450 during camphor hydroxylation? QM/MM studies of different electronic states of compound I and of reduced and oxidized iron−oxo intermediates. J. Am. Chem. Soc. *129*, 8978–8987. https://doi.org/10.1021/ja066847y.

63. Maihom, T., Choomwattana, S., Wannakao, S., Probst, M., and Limtrakul, J. (2016). Ethylene epoxidation with nitrous oxide over Fe–BTC metal–organic frameworks: a DFT study. ChemPhysChem *17*, 3416–3422. https://doi.org/10.1002/cphc.201600836.

64. Bols, M.L., Snyder, B.E.R., Rhoda, H.M., Cnudde, P., Fayad, G., Schoonheydt, R.A., Van Speybroeck, V., Solomon, E.I., and Sels, B.F. (2021). Coordination and activation of nitrous oxide by iron zeolites. Nat. Catal. *4*, 332–340. https://doi.org/10.1038/s41929-021-00602-4.

65. Gani, T.Z.H., and Kulik, H.J. (2018). Understanding and breaking scaling relations in single-site catalysis: methane to methanol conversion by FeIV=O. ACS Catal. *8*, 975–986. https://doi.org/10.1021/acscatal.7b03597.

66. Barona, M., and Snurr, R.Q. (2020). Exploring the tunability of trimetallic MOF nodes for partial oxidation of methane to methanol. ACS Appl. Mater. Interfaces *12*, 28217–28231. https://doi.org/10.1021/acsami.0c06241.

67. Rosen, A.S., Notestein, J.M., and Snurr, R.Q. (2019). Structure–activity relationships that identify metal–organic framework catalysts for methane activation. ACS Catal. *9*, 3576–3587. https://doi.org/10.1021/acscatal.8b05178.

68. Kulkarni, A.R., Zhao, Z.-J., Siahrostami, S., Nørskov, J.K., and Studt, F. (2018). Cation-exchanged zeolites for the selective oxidation of methane to methanol. Catal. Sci. Technol. *8*,

114–123. https://doi.org/10.1039/C7CY01229B.

69. Latimer, A.A., Kulkarni, A.R., Aljama, H., Montoya, J.H., Yoo, J.S., Tsai, C., Abild-Pedersen, F., Studt, F., and Nørskov, J.K. (2017). Understanding trends in C–H bond activation in heterogeneous catalysis. Nat. Mater. *16*, 225–229. https://doi.org/10.1038/nmat4760.

70. Hall, J.N., and Bollini, P. (2020). Low-temperature, ambient pressure oxidation of methane to methanol over every tri-iron node in a metal–organic framework. Chemistry (Basel). *26*, 16639–16643. https://doi.org/10.1002/chem.202003894.

71. Gkaniatsou, E., Sicard, C., Ricoux, R., Mahy, J.-P., Steunou, N., and Serre, C. (2017). Metal–organic frameworks: a novel host platform for enzymatic catalysis and detection. Mater. Horiz. *4*, 55–63. https://doi.org/10.1039/C6MH00312E.

72. Gkaniatsou, E., Ricoux, R., Kariyawasam, K., Stenger, I., Fan, B., Ayoub, N., Salas, S., Patriarche, G., Serre, C., Mahy, J.-P., et al. (2020). Encapsulation of microperoxidase-8 in MIL-101(Cr)-X nanoparticles: influence of metal–organic framework functionalization on enzymatic immobilization and catalytic activity. ACS Appl. Nano Mater. *3*, 3233–3243. https://doi.org/10.1021/acsanm.9b02464.

73. Baek, J., Rungtaweevoranit, B., Pei, X., Park, M., Fakra, S.C., Liu, Y.-S., Matheu, R., Alshmimri, S.A., Alshehri, S., Trickett, C.A., et al. (2018). Bioinspired metal–organic framework catalysts for selective methane oxidation to methanol. J. Am. Chem. Soc. *140*, 18208–18216. https://doi.org/10.1021/jacs.8b11525.

74. Yang, Y., and Arnold, F.H. (2021). Navigating the unnatural reaction space: directed evolution of heme proteins for selective carbene and nitrene transfer. Acc. Chem. Res. *54*, 1209–1225. https://doi.org/10.1021/acs.accounts.0c00591.

75. Onderko, E.L., Silakov, A., Yosca, T.H., and Green, M.T. (2017). Characterization of a selenocysteine-ligated P450 compound I reveals direct link between electron donation and reactivity. Nat. Chem. *9*, 623–628. https://doi.org/10.1038/nchem.2781.

76. Ganai, A., Ball, B., and Sarkar, P. (2023). Modulating the energetics of C–H bond activation in methane by utilizing metalated porphyrinic metal–organic frameworks. J. Phys. Chem. Lett. *14*, 1832–1839. https://doi.org/10.1021/acs.jpclett.2c03891.

77. Bara, D., Wilson, C., Mörtel, M., Khusniyarov, M.M., Ling, S., Slater, B., Sproules, S., and Forgan, R.S. (2019). Kinetic control of interpenetration in Fe–Biphenyl-4,4′-dicarboxylate metal–organic frameworks by coordination and oxidation modulation. J. Am. Chem. Soc. *141*, 8346–8357. https://doi.org/10.1021/jacs.9b03269.

78. Feng, D., Wang, K., Wei, Z., Chen, Y.-P., Simon, C.M., Arvapally, R.K., Martin, R.L., Bosch, M., Liu, T.-F., Fordham, S., et al. (2014). Kinetically tuned dimensional augmentation as a versatile synthetic route towards robust metal–organic frameworks. Nat. Commun. *5*, 5723. https://doi.org/10.1038/ncomms6723.

79. Frisch, M.J., Trucks, G.W., Schlegel, H.B., Scuseria, G.E., Robb, M.A., Cheeseman, J.R., Scalmani, G., Barone, V., Petersson, G.A., Nakatsuji, H., et al. (2016). Gaussian 16 Rev. B.01.

80. Zhao, Y., and Truhlar, D.G. (2008). The M06 suite of density functionals for main group thermochemistry, thermochemical kinetics, noncovalent interactions, excited states, and transition elements: two new functionals and systematic testing of four M06-class functionals and 12 other functionals. Theor. Chem. Acc. *120*, 215–241. https://doi.org/10.1007/s00214-007-0310-x.

81. Weigend, F. (2006). Accurate Coulomb-fitting basis sets for H to Rn. Phys. Chem. Chem. Phys. *8*, 1057–1065. https://doi.org/10.1039/B515623H.

82. Weigend, F., and Ahlrichs, R. (2005). Balanced basis sets of split valence, triple zeta valence and quadruple zeta valence quality for H to Rn: design and assessment of accuracy. Phys. Chem. Chem. Phys. *7*, 3297–3305. https://doi.org/10.1039/B508541A.

83. Vitillo, J.G., and Gagliardi, L. (2021). Modeling metal influence on the gate opening in ZIF-8 materials. Chem. Mater. *33*, 4465–4473. https://doi.org/10.1021/acs.chemmater.1c00623.

84. McCusker, K.P., and Klinman, J.P. (2010). An active-site phenylalanine directs substrate binding and C−H cleavage in the α-ketoglutarate-dependent dioxygenase TauD. J. Am. Chem. Soc. *132*, 5114–5120. https://doi.org/10.1021/ja909416z.

85. Mavrandonakis, A., Vogiatzis, K.D., Boese, A.D., Fink, K., Heine, T., and Klopper, W. (2015). Ab initio study of the adsorption of small molecules on metal–organic frameworks with oxo-centered trimetallic building units: the role of the undercoordinated metal ion. Inorg. Chem. *54*, 8251–8263. https://doi.org/10.1021/acs.inorgchem.5b00689.

86. Vitillo, J.G., and Gagliardi, L. (2021). Thermal treatment effect on CO and NO adsorption on Fe(II) and Fe(III) species in Fe(3)O-based MIL-type metal-organic frameworks: a density functional theory study. Inorg. Chem. *60*, 11813–11824. https://doi.org/10.1021/acs.inorgchem.1c01044.

87. Boys, S.F., and Bernardi, F. (1970). The calculation of small molecular interactions by the differences of separate total energies. Some procedures with reduced errors. Mol. Phys. *19*, 553–566.

88. Grimme, S. (2012). Supramolecular binding thermodynamics by dispersion-corrected density functional theory. Chem. Eur J. *18*, 9955–9964. https://doi.org/10.1002/chem.201200497.

89. Ribeiro, R.F., Marenich, A.V., Cramer, C.J., and Truhlar, D.G. (2011). Use of solution-phase vibrational frequencies in continuum models for the free energy of solvation. J. Phys. Chem. B *115*, 14556–14562. https://doi.org/10.1021/jp205508z.

90. Zhao, Y., and Truhlar, D.G. (2008). Computational characterization and modeling of buckyball tweezers: density functional study of concave-convex p···p interactions. Phys. Chem. Chem. Phys. *10*, 2813–2818. https://doi.org/10.1039/B717744E.

91. John, M., Alexopoulos, K., Reyniers, M.-F., and Marin, G.B. (2017). Mechanistic insights into the formation of butene isomers from 1-butanol in H-ZSM-5: DFT based microkinetic modelling. Catal. Sci. Technol. *7*, 1055–1072. https://doi.org/10.1039/C6CY02474B.

92. Isley, W., III (2018). G09-Quasiharmonic-Freq-Corrector.pl. https://github.com/william-isley-3rd/Comp-Chem-Tools.

93. Marenich, A.V., Jerome, S.V., Cramer, C.J., and Truhlar, D.G. (2012). Charge model 5: an extension of Hirshfeld population analysis for the accurate description of molecular interactions in gaseous and condensed phases. J. Chem. Theor. Comput. *8*, 527–541. https://doi.org/10.1021/ct200866d.

94. Ritchie, J.P., and Bachrach, S.M. (1987). Some methods and applications of electron density distribution analysis. J. Comput. Chem. *8*, 499–509. https://doi.org/10.1002/jcc.540080430.

95. Roos, B.O. (1987). The complete active space self-consistent field method and its applications in electronic structure calculations. In Advances in Chemical Physics, K.P. Lawley, ed. (Wiley & Sons), pp. 399–445. https://doi.org/10.1002/9780470142943.ch7.

96. Andersson, K., Malmqvist, P.A., Roos, B.O., Sadlej, A.J., and Wolinski, K. (1990). Second-order perturbation theory with a CASSCF reference function. J. Phys. Chem. *94*, 5483–5488. https://doi.org/10.1021/j100377a012.

97. Aquilante, F., Autschbach, J., Carlson, R.K., Chibotaru, L.F., Delcey, M.G., De Vico, L., Fdez Galván, I., Ferré, N., Frutos, L.M., Gagliardi, L., et al. (2016). Molcas 8: new capabilities for multiconfigurational quantum chemical calculations across the periodic table. J. Comput. Chem. *37*, 506–541. https://doi.org/10.1002/jcc.24221.

98. Roos, B.O., Lindh, R., Malmqvist, P.-Å., Veryazov, V., and Widmark, P.-O. (2005). New relativistic ANO basis sets for transition metal atoms. J. Phys. Chem. A *109*, 6575–6579. https://doi.org/10.1021/jp0581126.

99. Roos, B.O., Lindh, R., Malmqvist, P.Å., Veryazov, V., and Widmark, P.-O. (2004). Main group atoms and dimers studied with a new relativistic ANO basis set. J. Phys. Chem. A *108*, 2851–2858. https://doi.org/10.1021/jp031064.